

The interacting resonant level model in nonequilibrium: finite temperature effects

D.M. Kennes and V. Meden

*Institut für Theorie der Statistischen Physik, RWTH Aachen University and
JARA—Fundamentals of Future Information Technology, 52056 Aachen, Germany*

(Dated: November 9, 2019)

We study the steady-state properties as well as the relaxation dynamics of the nonequilibrium interacting resonant level model at finite temperatures. It constitutes the prototype model of a correlated charge fluctuating quantum dot. The two reservoirs are held at different chemical potentials—the difference being the bias voltage—and different temperatures; we discuss the transport through as well as the occupancy of the single level dot. First, we show analytically that in the steady state the reservoir temperatures in competition with the other energy scales act as infrared cutoffs. This is rather intuitive but, depending on the parameter regime under consideration, leads to a surprisingly rich variety of power laws in the current as a function of the temperatures and the bias voltage with different interaction dependent exponents. Next we clarify how finite reservoir temperatures affect the dynamics. They allow to tune the interplay of the two frequencies characterizing the oscillatory part of the time evolution of the model at zero temperature. For the exponentially decaying part we disentangle the contributions of the level-lead hybridization and the temperatures to the decay rates. We identify a coherent-to-incoherent transition in the long time dynamics as the temperature is raised. It occurs at an interaction dependent critical temperature. Finally, taking different temperatures in the reservoirs we discuss the relaxation dynamics of a temperature gradient driven current.

PACS numbers: 05.10.Cc, 05.60.Gg, 72.10.Fk, 73.63.Kv

I. INTRODUCTION

In recent years interacting nano-structures have attracted a great deal of both experimental as well as theoretical interest. They exhibit a variety of interesting many-body effects. Being equally fascinating and challenging to access theoretically, these systems are subject of a variety of studies (for a recent review see Ref. 1). An experimentally well controlled setup is given by a quantum dot featuring only a few electronic degrees of freedom contacted to a certain number of reservoirs. Due to the Coulomb repulsion these systems usually feature strong local electron correlations. A prominent consequence of those is the Kondo effect: if a nearly odd number of electrons reside on the quantum dot, spin fluctuations lead to a many-body resonance.² Besides of spin fluctuating quantum dot setups a typical model of interest is the interacting resonant level model (IRLM), which is dominated by charge fluctuations.^{3,4} The IRLM is given by a single level which is tunnel coupled to a certain number of reservoirs (leads) of spinless fermions. A particle occupying the dot level interacts with the reservoir fermions located close to the dot. The level is usually subject to an external gate voltage, which allows to tune its energy. Here we study the IRLM in a minimal transport setup with two reservoirs.

Currently the research focus shifts from the equilibrium to the nonequilibrium physics of quantum dots. One can aim at the bias voltage driven steady-state (which is usually assumed to exist) properties,^{5–14} or to be even more ambitious at the entire relaxation dynamics from transient to asymptotic.^{5,8,9,15,16} For the second task it is usually assumed that at some time t_0 the initially decoupled quantum dot is coupled to the leads and thus

relaxation from its initially prepared to its steady state sets in. In contrast to the well studied equilibrium properties, the nonequilibrium physics remains largely uncharted. In particular this holds if standard perturbative approaches fail to provide reliable results due to the presence of logarithmically divergent terms as it is the case in the IRLM.¹⁷ For such problems renormalization group (RG) approaches^{12,18,19} might succeed to describe the system under consideration.

Recently a functional RG (FRG) approach¹⁹ was developed to tackle the nonequilibrium properties of interacting quantum dots²⁰ and tested successfully in its application to the IRLM.^{17,21,22} Combined with studies using alternative methods^{23–29} this has led to a comprehensive understanding of the bias voltage driven steady state as well as the relaxation dynamics at vanishing temperature of the reservoirs. By far less is known about the physics at elevated temperatures.²³ Here we aim at closing this gap and present a detailed study of the nonequilibrium IRLM with finite reservoir temperatures using FRG. We discuss the steady state behavior as well as the dynamics at arbitrary (possibly asymmetric) temperatures in the reservoirs and for a general bias voltage. Our results are approximate, but controlled to leading order in the local electron-electron interaction; the RG procedure ensures that they are far superior to perturbation theory. Logarithms in the hopping amplitudes are resumed leading to power laws with interaction dependent exponents.^{3,4,17,21–25,30,31} We show that in the steady state the temperatures serve as infrared cutoff scales to the renormalization of these tunnel couplings and as such compete with the other low-energy scales. Although the temperature enters the renormalization in an intuitive way, depending on the parameter regime studied, the

competition leads to a surprisingly rich variety of power laws in the dependence of the current on the temperatures and the voltage with interaction dependent exponents. In the relaxation dynamics of the current and the occupancy varying the two temperatures allows to individually tune the amplitudes of the characteristic oscillatory terms and to vary the decay rates. We characterize a coherent-to-incoherent transition as the temperature is increased. At this the long time dynamics changes from being exponential with overlaid oscillations to being purely exponential. This transition takes place at a critical temperature which depends in a nontrivial way on the interaction strength. Finally, we investigate the time evolution of a current driven by a temperature gradient instead of a bias voltage.

The rest of our paper is structured as follows. In Sect. II we outline the model under consideration and additionally describe the FRG approach followed to tackle the problem at hand. Our result, first for the steady state analysis and then for the dynamics, are presented in Sect. III. We conclude our paper by a short summary in the final Sect. IV.

II. MODEL AND METHOD

A. Model

Our model is given by the Hamiltonian

$$H = H^{\text{dot}} + \sum_{\alpha=L,R} [H_{\alpha}^{\text{res}} + H_{\alpha}^{\text{coup}}]. \quad (1)$$

The dot part H^{dot} consists of a linear geometry of three lattice sites with

$$\begin{aligned} H_0^{\text{dot}} &= \epsilon n_2 - U \left(\frac{n_1}{2} + n_2 + \frac{n_3}{2} \right) \\ &\quad + (\tau_{12} d_1^{\dagger} d_2 + \tau_{23} d_2^{\dagger} d_3 + \text{H.c.}), \quad (2) \\ H^{\text{int}} &= U(n_1 n_2 + n_2 n_3), \quad (3) \end{aligned}$$

in standard second quantized notation. Here $n_j = d_j^{\dagger} d_j$ is the occupancy operator of the spinless fermionic level j . The levels (sites) are connected locally through a hopping amplitude $\tau_{ij} > 0$ and a Coulomb repulsion $U \geq 0$. The central site can be subject to a gate voltage allowing to tune the onsite energy ϵ . The second term in the single-particle part of the Hamiltonian is added such that $\epsilon = 0$ corresponds to half dot filling of the central dot site in equilibrium. The two leads $\alpha = L, R$ are modeled as noninteracting,

$$H_{\alpha}^{\text{res}} = \sum_{k_{\alpha}} \epsilon_{k_{\alpha}} c_{k_{\alpha}}^{\dagger} c_{k_{\alpha}}. \quad (4)$$

The left (right) lead is tunnel-coupled to side 1 (3) by

$$H_{\alpha}^{\text{coup}} = \gamma_{\alpha} \sum_{k_{\alpha}} c_{k_{\alpha}}^{\dagger} d_{j_{\alpha}} + \text{H.c.}, \quad (5)$$

with $j_L = 1$ and $j_R = 3$. For brevity we have not included time dependent parameters in H^{dot} and H^{int} which can also be treated by our approach as outlined in Ref. 32 for reservoir temperatures $T_{L/R} = 0$.

We assume that the system is prepared in a product density matrix state ρ at time $t_0 = 0$, which describes a situation naturally arising when the coupling between the dot and the reservoirs vanishes for $t < 0$. Furthermore, the reservoirs are in grand canonical equilibrium with $T_{\alpha} = 1/\beta_{\alpha}$ and chemical potentials centred around zero $\mu_L = -\mu_R = V/2 \geq 0$, that is

$$\rho(t=0) = \rho_0 = \rho_0^{\text{dot}} \otimes \rho_{L,0}^{\text{res}} \otimes \rho_{R,0}^{\text{res}}, \quad (6)$$

$$\rho_{\alpha,0}^{\text{res}} = e^{-(H_{\alpha}^{\text{res}} - \mu_{\alpha} N_{\alpha})/T_{\alpha}} / \text{Tr} e^{-(H_{\alpha}^{\text{res}} - \mu_{\alpha} N_{\alpha})/T_{\alpha}}, \quad (7)$$

where $N_{\alpha} = \sum_{k_{\alpha}} c_{k_{\alpha}}^{\dagger} c_{k_{\alpha}}$. We choose units with the Boltzmann constant $k_B = 1$, $\hbar = 1$, and electron charge $e = 1$. Finally, we assume that the statistical operator ρ_0^{dot} at $t = 0$ describes an initially empty quantum dot.

We aim at a limit in which the model is equivalent to the field theoretical IRLM.^{3,4,23–26,30,31} This is called the scaling limit and can be achieved by coupling the first and third site much stronger to their respective reservoirs than to the central site. It is then that the first and third dot sites can effectively be incorporated into the leads^{17,22} resulting in a single level (central site) tunnel coupled to and interacting with the reservoirs. We are interested in the universal physics which is independent of the details of the leads band structure. Therefore we study structureless reservoirs (wide band limit) with hybridization

$$\Gamma_{\alpha} = \pi D_{\alpha} |\gamma_{\alpha}|^2 \quad (8)$$

much larger than all other energy scales and constant density of states

$$D_{\alpha}(\epsilon) = D_{\alpha} e^{-\delta|\epsilon|}, \quad (9)$$

with $\delta \rightarrow 0^+$ assuring convergence of the energy integrals. For simplicity of depiction we will use symmetric couplings to the reservoirs of site one and three $\Gamma_{\alpha} = \Gamma$. In summary the limit $\tau_{ij}, |\epsilon|, |U|, V, |T_{\alpha}| \ll \Gamma$ establishes that the model is equivalent to the field theoretical IRLM.

B. Method

To analyse the behavior of the IRLM at finite reservoir temperatures we extend the methods described in Ref. 17 for the nonequilibrium steady state and Ref. 22 for the time evolution. We here give an outline of our approach and discuss the essential new steps. For a more detailed description of the FRG approaches we refer to the aforementioned publications.

To tackle the nonequilibrium problem at hand we employ the Keldysh formalism.^{33,34} In a two step procedure we first include the influence of the reservoirs on the non-interacting dot and secondly calculate the effect of the

two-particle interaction both in form of self-energy contributions. This yields the Dyson equation (in symbolic notation)

$$G^0 = g^0 + g^0 \Sigma_{\text{res}} G^0 \quad (10)$$

for the first step and

$$G = G^0 + G^0 \Sigma G \quad (11)$$

for the second one, with the noninteracting dot propagator g^0 (in Keldysh space), the reservoir dressed but still noninteracting propagator G^0 and the propagator of the full interacting system G . Internal multiplication in frequency space (steady state) and convolutions in time space (time evolution) are left implicit. The reservoir's self-energy Σ_{res} is calculated exactly, while the contribution of the two-particle interaction is determined via an approximate FRG approach.

The FRG is a method which allows to describe the physics of interacting quantum many-body systems exhibiting a hierarchy of energy scales and/or competing instabilities.¹⁹ First, one introduces a flow parameter Λ in the noninteracting part of the propagation, which for infrared divergent problems might be chosen to serve as an infrared cutoff. Consequently, one-particle irreducible vertex functions (effective interactions) acquire a cutoff dependence. Taking the derivative of the generating functional with respect to the latter yields an exact infinite hierarchy of flow equations for the vertex functions. To obtain a finite closed set of differential equations for the self-energy (single-particle vertex), the effective two-particle interaction (two-particle vertex), and possibly higher order vertex functions one truncates this hierarchy to a given order. The cutoff-free problem is recovered after integrating from $\Lambda = \infty$ (where the vertices are known analytically) down to $\Lambda = 0$. Note that the truncation is the only approximation, whereas the full dependences on the single-particle quantum numbers and the frequencies (steady state) or the times (time evolution) are kept. Here we use the lowest truncation order giving a frequency independent (steady state) or single time dependent (time evolution) self-energy. This simple truncation already allows to obtain a comprehensive understanding of the nonequilibrium physics of the IRLM at zero temperature and for small to intermediate interactions: the logarithmically divergent terms present in lowest-order perturbation theory are resummed consistently leading to RG-renormalized hopping amplitudes featuring generic power laws with interaction-dependent exponents. This in turn gives rise to many-body effects in observables such as current-voltage characteristics dominated by power laws with interaction-dependent exponents.^{17,21–25,27} Within the truncated FRG one obtains the latter to leading order in the interaction.¹⁷ For the time evolution FRG leads to terms exponentially decaying in time with interaction dependent decay rates as well as power-law corrections $t^{-\kappa}$ with U -dependent exponent²² κ also found in an alternative RG

procedure.^{21,27} The simplest truncation thus captures important characteristics of correlated charge fluctuations within the IRLM at $T_\alpha = 0$.

We specify the cutoff by coupling an auxiliary structureless reservoir held at infinite temperature to each of our three distinct lattice sites via hybridization Λ . For the $T = 0$ steady-state analysis the auxiliary reservoirs were held at vanishing chemical potential and temperature in earlier studies.^{17,21} We showed explicitly that infinite and zero temperature in the auxiliary reservoirs give the same results^{22,35} exemplifying the robustness of the cutoff procedure.

Finally the flow equation for the self-energy reads

$$\begin{aligned} \partial_\Lambda \gamma_1^\Lambda(\mathbb{1}, \mathbb{1}') &= \sum_{2,2'} [\hat{G}^\Lambda (\partial_\Lambda [\hat{G}^{0,\Lambda}]^{-1}) \hat{G}^\Lambda]_{2',2} \gamma_2(\mathbb{1}, 2, \mathbb{1}', 2') \\ &= - \sum_{2,2'} \hat{S}_{2',2}^\Lambda \gamma_2(\mathbb{1}, 2, \mathbb{1}', 2'), \end{aligned} \quad (12)$$

with the bare two-particle vertex γ_2 . We define the so-called ‘single-scale propagator’ as

$$\begin{aligned} \hat{S}_{11'}^\Lambda &= - \sum_{2,2'} \hat{G}_{12'}^\Lambda [\partial_\Lambda [\hat{G}^{0,\Lambda}]^{-1}]_{2',2} \hat{G}_{21'}^\Lambda \\ &= \partial_\Lambda^* \hat{G}_{11'}^\Lambda. \end{aligned} \quad (13)$$

We here introduced the star differential operator ∂_Λ^* which acts only on the free Green function $\hat{G}^{0,\Lambda}$, not on Σ^Λ , in the series expansion $\hat{G}^\Lambda = \hat{G}^{0,\Lambda} + \hat{G}^{0,\Lambda} \Sigma^\Lambda \hat{G}^{0,\Lambda} + \dots$. The internal sums run over the multi-index $\mathbb{1}, 2, \dots = (i, \omega, p)$ (steady state) or $\mathbb{1}, 2, \dots = (i, t, p)$ (time evolution) with the single-particle index i , the frequency ω , the time t and the Keldysh contour index p .

We emphasize two consequences of our truncation order. (i) During the flow no Keldysh self-energy is generated by the two-particle interaction. (ii) The self-energy originating from the two-particle interaction appears in combination with the single-particle part of the dot Hamiltonian in all equations. Thus, the former can be interpreted as a (for the time evolution time dependent) renormalization of the single-particle parameters (indicated by superscript Λ). This entails that conservation laws, such as charge conservation $\frac{d\bar{n}(t)}{dt} = J_L(t) + J_R(t)$ or simpler $J_L = -J_R$ in the steady state, where $\bar{n}(t)$ denotes the occupancy of the central dot site 2, are trivially fulfilled. In addition, one can formulate the flow equations in form of flowing single-particle parameters, which are the onsite energy of site one and three ϵ'^Λ (renormalize equally in our truncation), the onsite energy of the central site ϵ^Λ as well as the hopping between sites one and two τ_{12}^Λ and between two and three τ_{23}^Λ (generically renormalize differently in nonequilibrium).

Steady State—In contrast to the $T_\alpha = 0$ -study of Ref. 17 we employ the cutoff via auxiliary reservoirs featuring infinite temperature (instead of zero temperature; see above). The reservoir Keldysh self-energy takes the form

(in lattice site space)

$$\Sigma_{\text{res}}^K(\omega) = 4i\Gamma \begin{pmatrix} f_L(\omega) - 1/2 & 0 & 0 \\ 0 & 0 & 0 \\ 0 & 0 & f_R(\omega) - 1/2 \end{pmatrix} \quad (14)$$

with f_α being the Fermi function of reservoir α . The Keldysh Green function is then determined via

$$G^{K,\Lambda}(\omega) = G^{\text{ret},\Lambda}(\omega) \Sigma_{\text{res}}^K(\omega) G^{\text{adv},\Lambda}(\omega) \quad (15)$$

since the Keldysh self-energy from the two-particle interaction vanishes in our truncation. We can use unchanged expressions for retarded and advanced Green functions as compared to the $T = 0$ case;¹⁷ the temperature does not enter in these quantities explicitly. The single-scale propagator $S^{K,\Lambda}(\omega)$ is related to the Keldysh Green function by Eq. (13). As the latter depends on the T_α we have to account for finite temperature changes in the flow equations. Those read

$$\partial_\Lambda \tau_{12}^\Lambda = \frac{iU}{4\pi} \int S_{12}^{K,\Lambda}(\omega) d\omega \quad \tau_{12}^{\Lambda \rightarrow \infty} = \tau_{12} \quad (16)$$

$$\partial_\Lambda \tau_{23}^\Lambda = \frac{iU}{4\pi} \int S_{23}^{K,\Lambda}(\omega) d\omega \quad \tau_{23}^{\Lambda \rightarrow \infty} = \tau_{23} \quad (17)$$

$$\partial_\Lambda \epsilon^\Lambda = -\frac{iU}{4\pi} \int [S_{11}^{K,\Lambda} + S_{33}^{K,\Lambda}](\omega) d\omega \quad \epsilon^{\Lambda \rightarrow \infty} = \epsilon \quad (18)$$

$$\partial_\Lambda \epsilon'^\Lambda = -\frac{iU}{4\pi} \int S_{22}^{K,\Lambda}(\omega) d\omega \quad \epsilon'^{\Lambda \rightarrow \infty} = 0. \quad (19)$$

Time evolution—For the time evolution we generalize the method outlined in Ref. 22 to finite temperatures. Again we aim at the changes induced by the reservoir Keldysh self-energy, which enter the Keldysh Green function $G^K(t, t)$ and the single scale propagator $S^K(t, t)$. For this it is necessary to evaluate integrals of the type

$$\int dt \frac{e^{-at}}{\sinh(\pi T_\alpha t)} \quad (20)$$

which can be done analytically in form of polygamma $\Psi(n, x)$ and hypergeometric functions ${}_2F_1(a, b, c, z)$.³⁶ Since the formulas are rather lengthy, they are given in the Appendix.

III. RESULTS

A. Steady State

Temperature as a cutoff scale—At this point one can proceed with a numerical solution of the flow equations (16)-(19). We postpone this and first report on analytical results. To achieve those we suppress the renormalization of the central onsite energy ϵ^Λ which is $\mathcal{O}(U^2)$ (remind that in our truncation we only control terms to order U) as well as ϵ'^Λ , which always appears in combination with

the much larger scale Γ . This gives

$$\begin{aligned} \partial_\Lambda \tau_{12}^\Lambda &= -\frac{U\Gamma}{\pi} \int_{-\infty}^{\infty} \partial_\Lambda^* \left[G_{11}^{\text{ret},\Lambda}(\omega) (f_L(\omega) - 1/2) G_{12}^{\text{adv},\Lambda}(\omega) \right] d\omega \\ &\quad - \frac{U\Gamma}{\pi} \int_{-\infty}^{\infty} \partial_\Lambda^* \left[G_{13}^{\text{ret},\Lambda}(\omega) (f_R(\omega) - 1/2) G_{32}^{\text{adv},\Lambda}(\omega) \right] d\omega \end{aligned} \quad (21)$$

$$\begin{aligned} \partial_\Lambda \tau_{23}^\Lambda &= -\frac{U\Gamma}{\pi} \int_{-\infty}^{\infty} \partial_\Lambda^* \left[G_{21}^{\text{ret},\Lambda}(\omega) (f_L(\omega) - 1/2) G_{13}^{\text{adv},\Lambda}(\omega) \right] d\omega \\ &\quad - \frac{U\Gamma}{\pi} \int_{-\infty}^{\infty} \partial_\Lambda^* \left[G_{23}^{\text{ret},\Lambda}(\omega) (f_R(\omega) - 1/2) G_{33}^{\text{adv},\Lambda}(\omega) \right] d\omega \end{aligned} \quad (22)$$

as the remaining flow equations. From these expressions we can extract the corresponding flow equations of the level-lead hybridization $\Theta_{ij} = |\tau_{ij}|^2/\Gamma$ neglecting all terms $\mathcal{O}(1/\Gamma^2)$

$$\begin{aligned} \partial_\Lambda \Theta_{12}^\Lambda &= \frac{U}{2\pi\Gamma} \partial_\Lambda^* \int_{-\infty}^{\infty} \left[\tanh\left(\frac{\beta_L(\omega - \mu_L)}{2}\right) \right. \\ &\quad \times \left. \frac{\Theta_{12}^\Lambda}{\omega - \epsilon - i(\Lambda + \Theta_{12}^\Lambda + \Theta_{23}^\Lambda)} + \text{c.c.} \right] d\omega \end{aligned} \quad (23)$$

$$\partial_\Lambda \Theta_{23}^\Lambda = \partial_\Lambda \Theta_{12}^\Lambda (1 \leftrightarrow 3, L \leftrightarrow R). \quad (24)$$

In a good approximation one can neglect the renormalization of Θ_{12} and Θ_{23} in the denominator—denoted as approximation 1 in the following—and integrate Eq. (23) to

$$\begin{aligned} \partial_\Lambda \Theta_{12}^\Lambda &= -\frac{U}{\pi\Gamma} \Theta_{12}^\Lambda \\ &\quad \times \text{Re} \left\{ \frac{\beta_L}{\pi} \Psi\left(1, \frac{1}{2} - \frac{i}{\pi} \frac{\beta_L}{2} [\epsilon - \mu_L + i(\Lambda + \Theta_{12} + \Theta_{23})]\right) \right\}, \end{aligned} \quad (25)$$

with $\Psi(1, x)$ being the trigamma function. Additionally, setting $\Psi(1, 1/2 + x) \approx 1/(2/\pi^2 + x)$ for all $\text{Re}[x] > 0$ (ensuring the correct value at $x = 0$ as well as asymptotic behavior) for the right hand side of the flow equation—denoted as approximation 2 in the following—finally yields

$$\partial_\Lambda \Theta_{12}^\Lambda \approx -\frac{U}{\pi\Gamma} \Theta_{12} \frac{2(2T_L/\pi + \Lambda + \Theta_{12} + \Theta_{23})}{(2T_L/\pi + \Lambda + \Theta_{12} + \Theta_{23})^2 + [(\epsilon - \mu_L)/2]^2}. \quad (26)$$

After reintroducing the UV cutoff³⁷ one can integrate this equation analytically and obtains

$$\frac{\Theta_{12}^{\Lambda=0}}{\tau_{12}^2} \sim \begin{cases} (\tau_{12}^2)^{-2U/(\pi\Gamma) + \mathcal{O}(U^2)} & |\epsilon - \mu_L|, T_L \ll T_K \ll \Gamma \\ V^{-2U/(\pi\Gamma) + \mathcal{O}(U^2)} & |\epsilon|, T_K, T_L \ll V \ll \Gamma \\ |\epsilon|^{-2U/(\pi\Gamma) + \mathcal{O}(U^2)} & V, T_K, T_L \ll |\epsilon| \ll \Gamma \\ T_L^{-2U/(\pi\Gamma) + \mathcal{O}(U^2)} & |\epsilon - \mu_L|, T_K \ll T_L \ll \Gamma \end{cases} \quad (27)$$

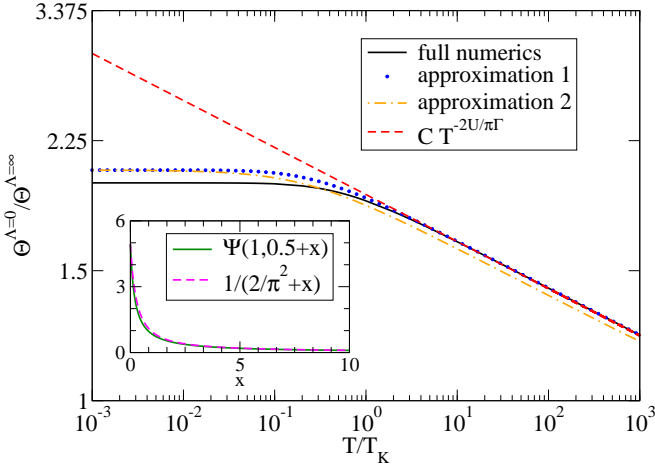


FIG. 1: (Color online) Renormalized line width $\Theta^{\Lambda=0}$ as a function of temperature T . Parameters are chosen as $\epsilon/T_K = V/T_K = 0$, $\tau_{12}/\Gamma = \tau_{23}/\Gamma = 0.0025$, $T = T_L = T_R$ and $U/\Gamma = 0.1$. Since left and right lead are chosen symmetrically $\Theta_{12} = \Theta_{23} = \Theta$ holds. Notice the double logarithmic scale, which indicates the power law behavior for large T . The inset shows the replacement of the trigamma function used in approximation 2.

with $\tau = \tau_{12} + \tau_{23}$ and T_K being the universal equilibrium low energy scale of the model^{3,4,23–26,30,31} defined via the charge susceptibility¹⁷

$$\chi = \left. \frac{d\bar{n}}{d\epsilon} \right|_{\epsilon=0} = -\frac{2}{\pi T_K}. \quad (28)$$

Equations analogous to (25)–(27) are obtained for the renormalization of $\Theta_{23}^{\Lambda=0}$ by replacing $(1 \rightarrow 3, L \rightarrow R)$. It is apparent that the reservoir temperatures indeed provide IR cutoffs as usually assumed [see Eq. (27)]. Equation (26) indicates the interplay of the different cutoff scales $\epsilon - \mu_\alpha$, $\Theta_{12} + \Theta_{23}$, T_α entering in the denominator explicitly. We find that the left (right) hybridization is cutoff by the temperature of the left (right) reservoir only. This invokes important consequences for the behavior of the current outlined in more detail in the next section. Different cutoff scales for the left and right hybridization have been observed before; it is $|\epsilon - \mu_L|$ ($|\epsilon - \mu_R|$) and not $V = \mu_L - \mu_R$ which might enter as a cutoff for Θ_{12} (Θ_{23}).²¹

We next elaborate on the quality of the approximations 1 and 2. To this end we take the full numerical solution of the flow equations (the only approximation being the truncation) and step by step apply approximations 1 and 2. A comparison for the renormalized line width $\Theta^{\Lambda=0}$ as a function of temperature is shown in Fig. 1. For the entire temperature range ($T_L = T_R = T$ and $\tau_{12} = \tau_{23} = \tau$ for simplicity) the results of approximations 1 and 2 agree well with the numerical solution. In particular for $T \gtrsim T_K$, the power law Eq. (27) with the correct exponent is reproduced on each level of approximation.

Observables—Within our truncation the effect of the interaction can be cast into effective single-particle parameters. To gain analytical insights it is therefore sufficient

to derive expressions for the occupancy and the current at vanishing interaction. One can simply supplement the noninteracting formulas with the effective parameters obtained at the end of the flow to incorporate the interaction. We focus on the current which is the most interesting observable in our transport setup. We start from the Meir-Wingreen form³⁸

$$J_L = 4\Gamma^2 \int d\omega [f_L(\omega) - f_R(\omega)] |G_{13}^{\text{ret}, \Lambda=0}|^2 \\ \approx 4\Theta_{12}^{\Lambda=0}\Theta_{23}^{\Lambda=0} \int d\omega [f_L(\omega) - f_R(\omega)] \\ \times \left| \frac{1}{i\omega - i\epsilon - \Theta_{12}^{\Lambda=0} - \Theta_{23}^{\Lambda=0}} \right|^2, \quad (29)$$

where terms $\mathcal{O}(U^2)$ (which we do not control in any case) as well as $\mathcal{O}(1/\Gamma^2)$ (scaling limit) were neglected in the second step. The integral can be solved and yields

$$J_L = 4 \frac{\Theta_{12}^{\Lambda=0}\Theta_{23}^{\Lambda=0}}{\Theta_{12}^{\Lambda=0} + \Theta_{23}^{\Lambda=0}} \sum_{p=L,R} s(p) \\ \times \text{Im} \left[\Psi \left(\frac{1}{2} - \frac{\beta_p}{2\pi} (i(\mu_p - \epsilon) - (\Theta_{12}^{\Lambda=0} + \Theta_{23}^{\Lambda=0})) \right) \right] \quad (30)$$

with $\Psi(x)$ being the digamma function, $s(L) = -1$ and $s(R) = 1$. Combining this expression with the flow Eq. (25) and its analogue for $\Theta_{23}^{\Lambda=0}$ allows us to obtain a comprehensive analytical understanding of the steady-state current.

In the ohmic regime (in which the current depends linearly on the voltage), for $T_L = T_R = T$, $\tau_{12} = \tau_{23} = \tau$, and at low T where $T_K \gg T, V, |\epsilon|$ the T -dependence of the current was earlier studied in Ref. 23 using a field theoretical approach. In this limit we find

$$\Theta_{12}^{\Lambda=0} = \Theta_{23}^{\Lambda=0} = \Theta_{12} \left(\frac{\Gamma}{T_K} \right)^{\frac{2U}{\Gamma\pi}} \exp \left[-\frac{2U}{\Gamma\pi} \left(\frac{\bar{T}^2}{6} - \frac{7\bar{T}^4}{60} \right) \right], \quad (31)$$

where we neglected terms $\mathcal{O}(\bar{T}^6)$ with $\bar{T} = \pi T/T_K$. Plugging the renormalized hybridizations into the current formula (30) yields

$$\frac{J_L}{V} = 1 - \frac{1}{3}\bar{T}^2 + \left(\frac{7}{15} - \frac{2U}{9\Gamma\pi} \right) \bar{T}^4 \quad (32)$$

up to $\mathcal{O}(\bar{T}^6)$ and $\mathcal{O}(U^2)$. The ratio $R = g_4/g_2^2$ of the prefactors of \bar{T}^2 (g_2) and \bar{T}^4 (g_4) is given by $R = 21/5 - 2U/\Gamma\pi$, which is the same result as found in Ref. 23 (see also Ref. 39).

At $T_{L/R} = 0$, for left-right symmetric tunnel couplings, $\epsilon = 0$ and for sufficiently large bias voltages Eq. (27) leads to a power-law suppression $J_L \sim V^{-\nu}$ of the current with $\nu = -\frac{2U}{\pi\Gamma}$.^{23–25} It was later shown^{21,27} that relaxing the second and/or third requirement leads to a more complicated form of the current-voltage characteristics. Allowing for a left-right asymmetry in the reservoir's temperatures (which is analogous to tuning V and ϵ) introduces

another level of complexity. We break it up by considering the symmetric case $T_\alpha = T \gg |\epsilon - \mu_\alpha|, T_K$, first. In this regime the flow of both level-lead couplings is cutoff by the temperature and the current reads

$$J_L \sim T^{-\frac{2U}{\pi\Gamma}-1}, \quad (33)$$

as long as $V \neq 0$ or $\epsilon \neq 0$. We emphasize that the exponent is different from the above given ν appearing in the voltage dependence. For $V = 0$ and $\epsilon = 0$, $J_L = 0$ independent of the temperature difference in the reservoirs. This follows right away from half filling. In the regime $T_L \gg T_R \gg |\epsilon - \mu_\alpha|, T_K$,

$$J_L \sim (T_L T_R)^{-\frac{2U}{\pi\Gamma}-1} \frac{c_2 T_L + T_R}{T_L^{-\frac{2U}{\pi\Gamma}} + c_1 T_R^{-\frac{2U}{\pi\Gamma}}}, \quad (34)$$

where c_1 stems from the asymmetry in the renormalization of the left and right hoppings (the exact form of c_1 is irrelevant for the following discussion) and $c_2 = -(\epsilon - V/2)/(\epsilon + V/2)$. Off resonance ($\epsilon \neq V/2$) the current is given by

$$J_L \sim (T_L T_R)^{-\frac{2U}{\pi\Gamma}-1} \frac{T_L}{T_L^{-\frac{2U}{\pi\Gamma}} + c_1 T_R^{-\frac{2U}{\pi\Gamma}}}, \quad (35)$$

but on resonance^{21,27} ($\epsilon = V/2$) it changes to

$$J_L \sim (T_L T_R)^{-\frac{2U}{\pi\Gamma}-1} \frac{T_R}{T_L^{-\frac{2U}{\pi\Gamma}} + c_1 T_R^{-\frac{2U}{\pi\Gamma}}}. \quad (36)$$

Similarly one finds for $T_L \gg V \gg T_R, |\epsilon|, T_K$,

$$J_L \sim \frac{(T_L V)^{-\frac{2U}{\pi\Gamma}}}{T_L^{-\frac{2U}{\pi\Gamma}} + c_1 V^{-\frac{2U}{\pi\Gamma}}}. \quad (37)$$

This exemplifies how the temperature significantly changes the qualitative behavior of the current, although it enters the renormalization of the hybridizations in an (“simple”) intuitive way (as an infrared cutoff).

B. Time evolution

The noninteracting case—To gain a comprehensive understanding of the effect of finite reservoir temperatures on the relaxation dynamics of the IRLM it is advantageous to first study the noninteracting case. In this limit closed analytical expressions for the time dependence of the current and occupancy can be obtained and the effect of $T_\alpha > 0$ on the relaxation rates and characteristic oscillations can be worked out in detail. A comparison with the $U > 0$ results obtained numerically by solving the FRG flow equations and computing $\bar{n}(t)$ and $J_L(t)$ then allows to assess the correlation effects. It was earlier shown that for $T_\alpha = 0$ and $|\epsilon - V/2| \gg T_K$ the relaxation dynamics for $U > 0$ and sufficiently large times can be obtained by replacing the time-independent bare parameters in analytical $U = 0$ expressions by the time-averaged renormalized single-particle parameters.²² Via this route the correlation effects become rather transparent. We show that the same holds for finite reservoir temperatures. The $U = 0$ expressions derived next are thus also of interest in this respect.

We introduce the hybridization of the single-level model $\tilde{\Gamma}_{ij}$. To connect to the three site model in the scaling limit one has to set

$$\tilde{\Gamma}_{ij} = \frac{|\tau_{ij}|^2}{\Gamma}. \quad (38)$$

For simplicity we focus on the case of symmetric couplings to the reservoirs $\tilde{\Gamma}_{ij} = \tilde{\Gamma}$. The occupancy $\bar{n}(t)$ with the initial value \bar{n}_0 reads (for expressions of the occupancy in terms of Green functions see Ref. 22)

$$\begin{aligned} \bar{n}(t) = & \frac{1}{2} - \frac{1}{2} e^{-4\tilde{\Gamma}t} (1 - 2\bar{n}_0) + \frac{1}{2} \sum_\alpha T_\alpha \text{Im} \left\{ \frac{1}{\pi T_\alpha} \Psi \left(\frac{-(i(\epsilon - \mu_\alpha) - 2\tilde{\Gamma} - \pi T_\alpha)}{2\pi T_\alpha} \right) - e^{-4\tilde{\Gamma}t} \frac{1}{\pi T_\alpha} \Psi \left(\frac{-(i(\epsilon - \mu_\alpha) + 2\tilde{\Gamma} - \pi T_\alpha)}{2\pi T_\alpha} \right) \right. \\ & - \frac{2e^{(i(\epsilon - \mu_\alpha) - 2\tilde{\Gamma} - \pi T_\alpha)t}}{(i(\epsilon - \mu_\alpha) - 2\tilde{\Gamma} - \pi T_\alpha)} {}_2\mathcal{F}_1 \left[1, \frac{-(i(\epsilon - \mu_\alpha) - 2\tilde{\Gamma} - \pi T_\alpha)}{2\pi T_\alpha}, \frac{-(i(\epsilon - \mu_\alpha) - 2\tilde{\Gamma} - \pi T_\alpha)}{2\pi T_\alpha} + 1, e^{-2\pi T_\alpha t} \right] \\ & \left. + \frac{2e^{(i(\epsilon - \mu_\alpha) - 2\tilde{\Gamma} - \pi T_\alpha)t}}{(i(\epsilon - \mu_\alpha) + 2\tilde{\Gamma} - \pi T_\alpha)} {}_2\mathcal{F}_1 \left[1, \frac{-(i(\epsilon - \mu_\alpha) + 2\tilde{\Gamma} - \pi T_\alpha)}{2\pi T_\alpha}, \frac{-(i(\epsilon - \mu_\alpha) + 2\tilde{\Gamma} - \pi T_\alpha)}{2\pi T_\alpha} + 1, e^{-2\pi T_\alpha t} \right] \right\}. \end{aligned} \quad (39)$$

Interestingly, the rate $4\tilde{\Gamma}$ appearing in the first exponential term remains independent of the temperatures. For

the time dependence of the current we find (for equations expressing the current in terms of Green functions

we again refer to Ref. 22)

$$\begin{aligned} \frac{J_L(t)}{\tilde{\Gamma}} = & 1 - 2\bar{n}(t) + 4T_L \frac{\text{Im} \left[\Psi \left(\frac{i(\mu_L - \epsilon) + 2\tilde{\Gamma} + \pi T_L}{2\pi T_L} \right) \right]}{2\pi T_L} \\ & - 4T_L \text{Re} \left\{ i \frac{e^{-(i(\mu_L - \epsilon) + 2\tilde{\Gamma} + \pi T_L)t}}{i(\mu_L - \epsilon) + 2\tilde{\Gamma} + \pi T_L} {}_2F_1 \left[1, \frac{i(\mu_L - \epsilon) + 2\tilde{\Gamma} + \pi T_L}{2\pi T_\alpha}, \frac{-(i(\epsilon - \mu_\alpha) + 2\tilde{\Gamma} - \pi T_\alpha)}{2\pi T_\alpha} + 1, e^{-2\pi T_\alpha t} \right] \right\}. \end{aligned} \quad (40)$$

Up to the above mentioned first time dependent term in $\bar{n}(t)$, which remains unchanged if T_α is increased, the dynamics is affected by the reservoir temperatures [e.g. compare to Eqs. (109)-(111) of Ref. 27]. The long-time behavior of the remaining terms in $\bar{n}(t)$ and $J_L(t)$ changes from being governed by an exponential relaxation in combination with a power-law correction for $T = 0$ ^{21,22,27} to an infinite series of exponential terms with temperature dependent rates $2\tilde{\Gamma} + 2n\pi T_\alpha$ and $n \in \mathbb{N}$ at $T > 0$. The frequencies characterising the oscillatory part of the behavior of $\bar{n}(t)$ and $J_L(t)$ are the same as for $T = 0$ ^{22,27} in general one finds the frequencies $|\epsilon \pm V/2|$, where the amplitude of $|\epsilon + V/2|$ ($|\epsilon - V/2|$) is suppressed in the regime $|\epsilon - V/2| \gg T_K$ in the current J_L (J_R).

Obviously the reservoir temperatures do not play the same role as the hybridisation (remind that $\tilde{\Gamma}_{12} = \tilde{\Gamma}_{23} = \tilde{\Gamma}$). In contrast to the latter, which enters in every relaxation rate of Eqs. (39) and (40), the temperature allows to tune the influence of the different terms with respect to each other; the rates dependent solely on either T_L or on T_R . Furthermore, even with asymmetric couplings to the left and right reservoir, that is generalizing Eqs. (39) and (40), only the sum of the hybridisations enter the decay rates. The temperatures instead allow to tune the relaxation rates imprinted by the left and right reservoir independently.

The interacting case—In the developed FRG approach we determine the Keldysh and retarded Green functions of the interacting system. Given those we can numerically compute the observables as outlined in Ref. 22. We postpone this and first consider the renormalization of the time dependent effective single-particle parameters. When combined with Eqs. (39) and (40) the latter give valuable insights in the effect of the two-particle interaction (see above as well as the discussion below). Figure 2 shows the renormalized onsite energy $\epsilon^{\Lambda=0}(t) - \epsilon = \Sigma_{22}^{\text{ret}, \Lambda=0} \in \mathbb{R}$ (note the double logarithmic scale) for different reservoir temperatures ($\tau_{12} = \tau_{23} = \tau$ for simplicity). For times $T_K t \gtrsim \tau/\Gamma$, the renormalization is of order U^2 (which we do not control) for all temperatures and thus negligibly small. Remarkably different temperature curves for the renormalization of the onsite energy collapse onto one universal curve (even on a logarithmic scale) as long as T is not too large.

The time dependence of the renormalized hopping am-

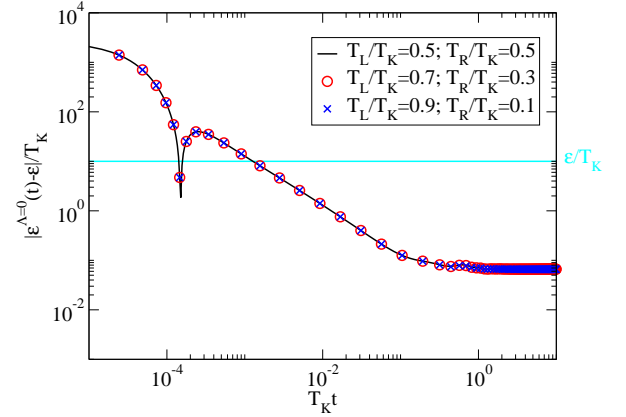


FIG. 2: (Color online) Time dependence of the renormalized onsite energy $\epsilon^{\Lambda=0}(t) - \epsilon \in \mathbb{R}$ (of the central site 2). The parameters are: $\tau_{12} = \tau_{23} = \tau$ with $\tau/\Gamma = 0.0025$, $\epsilon/T_K = V/T_K = 10$, and $U/\Gamma = 0.2$. Note the double logarithmic scale and that the dip corresponds to a zero crossing. It occurs in the non-universal regime $t \sim 1/\Gamma$

plitudes is shown in Fig. 3 (again for $\tau_{12} = \tau_{23} = \tau$). The renormalization of the hopping amplitude depends only weakly on the temperature for the considered case of large $|\epsilon - V/2|$. As for $T = 0$ ²² the renormalized hopping amplitudes quickly (on a scale $T_K t \sim \tau/\Gamma$) start to oscillate around their steady state values with frequencies $|\epsilon - V/2|$ and $|\epsilon + V/2|$ for $\tau_{12}^{\Lambda=0}$ and $\tau_{23}^{\Lambda=0}$ respectively. Note that due to the left-right asymmetry induced by the voltage and different reservoir temperatures the renormalized level-lead couplings generically differ even for the bare ones being equal. Increasing the temperature of the left (right) reservoir suppresses oscillations in the renormalized $\tau_{12}^{\Lambda=0}$ ($\tau_{23}^{\Lambda=0}$). For the sake of simplicity we only show the real part at this point, but the same holds for the much smaller imaginary one as well.

The analysis of the time dependence of the renormalized single-particle parameters in the limit $|\epsilon - V/2| \gg T_K$ shows that to interpret the results obtained by the numerical solution of the FRG flow equations and numerical computation of the observables for $T_K t \gtrsim \tau/\Gamma$ one can refer to Eqs. (39) and (40) with the bare parameters replaced by the time-averaged renormalized ones. More

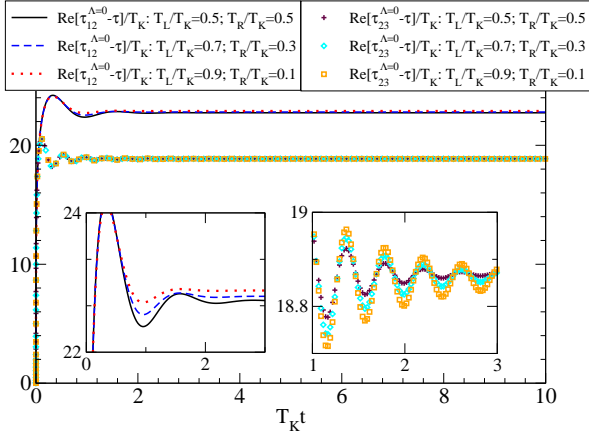


FIG. 3: (Color online) The same as in Fig. 2 but for the renormalized hoppings $\tau_{12}^{\Lambda=0} - \tau = \Sigma_{12}^{\text{ret}, \Lambda=0} \in \mathbb{C}$ between sites 1 and 2, and $\tau_{23}^{\Lambda=0} - \tau = \Sigma_{23}^{\text{ret}, \Lambda=0} \in \mathbb{C}$ between sites 2 and 3. The inset shows a zoom into the regime where one can most clearly distinguish the temperature's effect on the oscillations' amplitude.

precisely we have to extend these expressions to the case of left-right asymmetric hybridizations. For brevity we do not give those here but comment that the ratio of the hybridizations enters as prefactors in the different terms. Going one step further the oscillatory behavior of the renormalized hopping amplitudes with frequencies $|\epsilon \pm V/2|$ (see Fig. 3) can be taken into account as an interaction and temperature dependent phase.

We now discuss our numerical FRG results for $\bar{n}(t)$ and $J_L(t)$ at $U > 0$. To understand those we use the just developed relation to the noninteracting dynamics. Figures 4 and 5 show the time evolution of the occupancy and the current in the limit $|\epsilon - V/2| \gg T_K$ for different U . Obviously, the interacting system behaves quite similar to the noninteracting one as suggested from our study of the effective parameters and the earlier study at $T = 0$.^{21,22,27} Furthermore, one can see how increasing the temperature drastically suppresses the amplitude of the oscillatory terms. The quality factor is decreased by the increased decay rate. One can tune the quality factor of the two frequencies $|\epsilon \pm V/2|$ independently of each other, which is not possible via the hybridization. Figure 6 illustrates this point for the time dependence of the occupancy. For vanishing temperature gradient $\Delta T = 0$ it shows a superposition of the two frequencies $|\epsilon \pm V/2|$ (bottom curve in Fig. 6). Raising the temperature gradient pronounces the contribution of the frequency $|\epsilon + V/2|$ belonging to the colder reservoir until the signal appears almost sinusoidal (overlayed by an exponential decay) at maximum temperature gradient (top curve in Fig. 6). The inset shows the imaginary part of the numerical Laplace transform (normalized to its largest value) of the occupancy for the smallest and largest temperature gradient. The positions of the frequencies $|\epsilon \pm V/2|$ are indicated by the vertical arrows. With increasing ΔT the

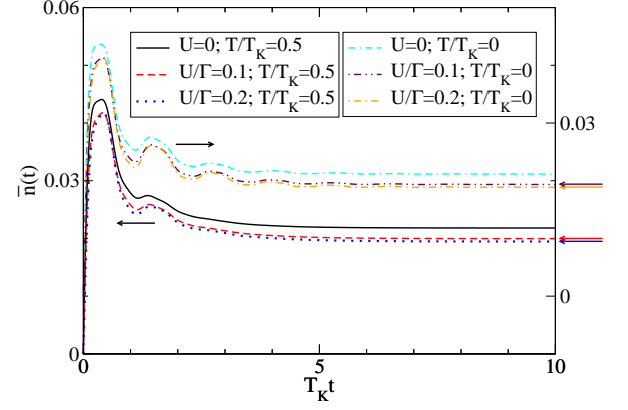


FIG. 4: (Color online) FRG data for the time evolution of the central-site occupancy. The parameters are the same as in Fig. 2 and symmetric temperatures $T_\alpha = T$. The arrows right to the graph indicate the steady-state values obtained by the nonequilibrium steady-state functional RG discussed earlier.

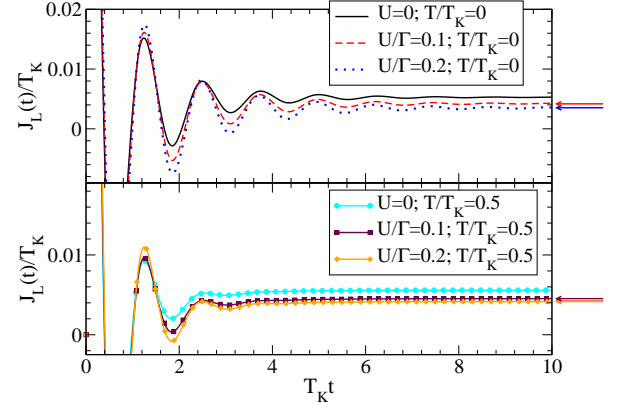


FIG. 5: (Color online) The same as in Fig. 4 but for the current leaving the left reservoir.

feature at $|\epsilon - V/2|$ is suppressed, while the one at $|\epsilon + V/2|$ is enhanced.

Next we study the far-from-equilibrium case $V \gg T_K, \epsilon = 0$, which on general grounds is the most intriguing one. More precisely we consider the limit $V \gg T_K, T$ with $T_L = T_R = T$ and $\epsilon = 0$. At $\epsilon = 0$ the expressions for the time evolution are particularly simple and for sufficiently large times $\pi T t \gg 1$ and small interactions we obtain

$$J_L(t) = J_{\text{stat}} + e^{-4\Theta^{\Lambda=0}t} - 2T \text{Im} \left[\frac{4e^{(-iV/2 - 2\Theta^{\Lambda=0} - \pi T)t}}{iV + 4\Theta^{\Lambda=0} + 2\pi T} \right], \quad (41)$$

with the renormalized steady-state values $\Theta^{\Lambda=0} = \Theta_{12}^{\Lambda=0} = \Theta_{23}^{\Lambda=0}$ and the stationary current J_{stat} . We note that for initially equal Θ_{ij} and $\epsilon = 0$ also the renormalized hybridizations remain equal even for $V \neq 0$. From Eq. (41) we can read off a coherent-to-incoherent transition in the

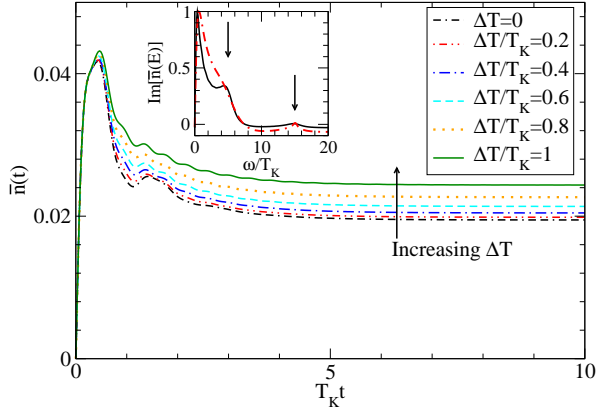


FIG. 6: (Color online) The same as Fig. 4 with $U/\Gamma = 0.2$, but featuring a temperature gradient $T_L = T + \Delta T/2$ and $T_R = T - \Delta T/2$ for $T = 0.5T_K$. We can find how the temperature gradient pronounces the frequency $|\epsilon + V/2|$ belonging to the colder reservoir. This can also be found in the inset, which shows the numerical Laplace transform with the positions of the frequencies $|\epsilon \pm V/2|$ indicated by arrows.

long-time dynamics at temperature

$$\pi T_c = 2\Theta^{\Lambda=0}. \quad (42)$$

The long time dynamics switches from being exponential with an overlaid oscillation (second term of Eq. (41) being the dominate one at large times) for $T < T_c$ to purely (monotonic) exponential relaxation (first term of Eq. (41) being the dominate one at large times) for $T > T_c$. To determine T_c we can take the expression for $\Theta^{\Lambda=0}$ corresponding to the considered parameter regime $V \gg T_K, T$ of Eq. (27) $\Theta^{\Lambda=0} \sim \frac{\tau^2}{\Gamma} \left(\frac{\Gamma}{V}\right)^{2U/\pi/\Gamma}$. With this we obtain

$$T_c = \frac{2\tau^2}{\pi\Gamma} \left(\frac{\Gamma}{V}\right)^{2U/\pi/\Gamma}. \quad (43)$$

The coherent-to-incoherent transition of the current dynamics is depicted in Fig. 7 for $U/\Gamma = 0.05$ (full numerical solution of the FRG flow equations).

We close the discussion by considering the time dependence of a current which is not induced by a finite bias voltage but by a finite temperature gradient across the quantum dot. To obtain a nonvanishing steady-state value of the current one needs to choose $\epsilon \neq 0$. Figure 8 shows the current for this parameter regime. Note that the only frequency in the time evolution is given by ϵ as $V = 0$. The interaction strength enhances the amplitude of the oscillations, but decreases the steady-state current (if measured with respect to T_K). This investigation opens the road to thermal and thermoelectric transport studies which will be presented elsewhere.

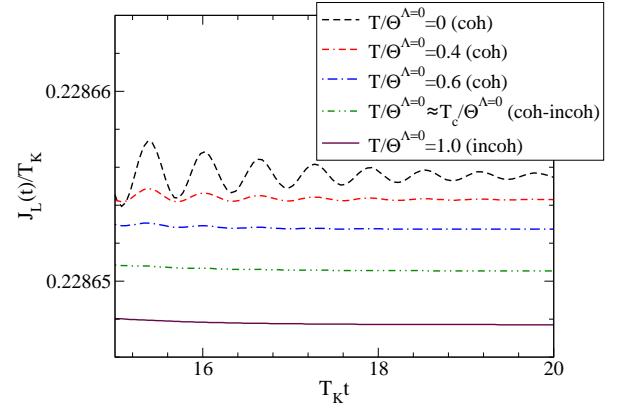


FIG. 7: (Color online) The coherent-to-incoherent transition described by (42). The parameters are $\tau/\Gamma = 0.0025$, $\epsilon/T_K = 0$, $V/T_K = 20$, and $U/\Gamma = 0.05$. We choose $T_\alpha = T$ and thus one finds the transition at $T/\Theta^{\Lambda=0} \approx 0.8028$.

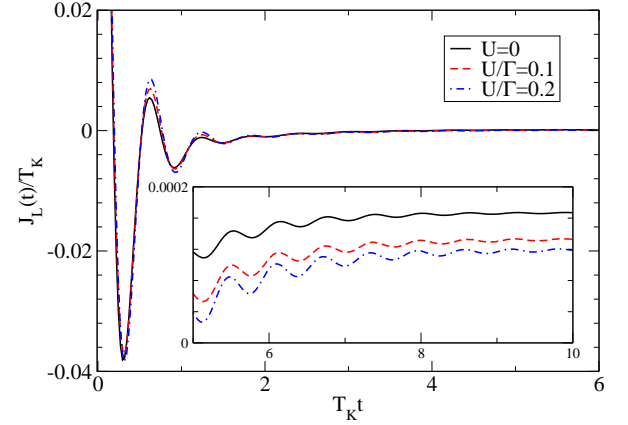


FIG. 8: (Color online) Time evolution for the temperature gradient induced current leaving the left reservoir $J_L(t)$. The parameters read $\tau/\Gamma = 0.0025$, $\epsilon/T_K = 10$ and $V/T_K = 0$. We choose $T_L = T_K$ and $T_R = 0$.

IV. SUMMARY

We extended the functional RG analysis of the nonequilibrium interacting resonant level model in the scaling limit, which is the prototype of a simple charge fluctuating quantum dot, to the case of arbitrary reservoir temperatures. Our study includes all time regimes from transient to asymptotic with the ultimate limit of the steady state. All results developed are controlled to leading order in the interaction, but known to be far superior to simple perturbation theory as our RG procedure implies the resummation of logarithmically divergent terms to power laws.

First we discussed the role of temperature as an RG cutoff competing with the other energy scales of the model in the steady state. Although the temperature enters the renormalization of the hybridization in an intuitive way, the current was shown to exhibit a vast variety

of different power laws (in temperature and bias voltage) with interaction dependent exponents for different parameter regimes. We then clarified the role of finite temperatures for the relaxation dynamics. We focused on the most transparent case $|\epsilon - V/2| \gg T_K, T_L, T_R$ in which the physics of the IRLM can be understood by interpreting the interacting system as an effective free one featuring renormalized parameters. The finite reservoir temperatures T_α (only) partly act similar to the hybridizations; increasing T_α increases the relaxation rate. Our detailed analysis shows that this obvious effect does not exhaust the role of temperature in the relaxation dynamics. We have shown explicitly that one can use the T_α to suppress the oscillatory contributions to the occupancy with the frequencies $|\epsilon \pm V/2|$ individually which is impossible by varying the hybridizations. We characterized a coherent-to-incoherent transition in the long-time relaxation dynamics as the temperature is increased. The critical temperature at which the transition occurs depends in a nontrivial way on the two-particle interaction. Finally, we discussed a current, which is not driven by a bias voltage, but by a temperature gradient. We emphasize that, similar to the $T = 0$ case, our approach can also be used

to tackle explicitly time-dependent Hamiltonians, which constitutes a field of current interest. A direction of future research which opens up directly from the present work is the field of thermal and thermoelectric transport. In this context quantum dots are promising candidates for highly efficient energy conversion devices and thus have recently gained sizeable interest.^{40–43}

Acknowledgments

We thank Dirk Schuricht for very valuable discussions and Frank Reininghaus for providing a numerical implementation of the complex trigamma function. This work was supported by the DFG via FOR 723.

Appendix

In the main part of this work it was discussed, that one needs to calculate the Keldysh Green function $G^K(t, t)$. It is determined by the integral

$$\int_{t_n}^{t_{n+1}} ds_1 \int_{t_m}^{t_{m+1}} ds_2 G^{\text{ret}}(t_{n+1}, s_1) \Sigma_{\text{res}}^K(s_1, s_2) G^{\text{adv}}(s_2, t_{m+1}) \quad (\text{A.1})$$

with $\Sigma_{\text{res}}^K(s_1, s_2)$ given by

$$\Sigma_{\alpha}^K(t', t) = \Gamma \begin{pmatrix} -T_L e^{-i\mu_L(t'-t)} \sum_{\pm} \frac{1}{\sinh[\pi T_L(t'-t \pm i\delta)]}, & 0 \\ 0 & 0 \\ 0 & -T_R e^{-i\mu_R(t'-t)} \sum_{\pm} \frac{1}{\sinh[\pi T_R(t'-t \pm i\delta)]} \end{pmatrix}. \quad (\text{A.2})$$

The retarded Green function can be evaluated as in the $T = 0$ case via

$$G_{ij}^{\text{ret}}(t, t') = -i \sum_{l=1}^3 \text{Res}_{ij,l} e^{-i\omega_l(t-t')}, \quad (\text{A.3})$$

with $\text{Res}_{ij,l}$ and ω_l being the residues and the poles of

$$\frac{1}{\omega - (\tilde{h}_0^{\text{dot}} + \Sigma_{\text{res}}^{\text{ret}} - i\Lambda + \Sigma_{\tilde{t}}^{\text{ret}})}. \quad (\text{A.4})$$

Introducing the time dependent effective parameters $\epsilon'^{\Lambda} = \Sigma_{\tilde{t},11}^{\text{ret}} - U/2$, $\epsilon^{\Lambda} = \epsilon + \Sigma_{\tilde{t},22}^{\text{ret}} - U$, $\tau_{12}^{\Lambda} = \tau + \Sigma_{\tilde{t},12}^{\text{ret}}$ and $\tau_{23}^{\Lambda} = \tau + \Sigma_{\tilde{t},23}^{\text{ret}}$ allows to express the poles as

$$\omega_1 = \epsilon'^{\Lambda} - i(\Gamma + \Lambda), \quad \omega_{2/3} = \frac{1}{2} \left(\epsilon^{\Lambda} + \epsilon'^{\Lambda} - i\Gamma - 2i\Lambda \mp \sqrt{-(\Gamma - i\epsilon^{\Lambda} + i\epsilon'^{\Lambda})^2 + 4|\tau_{12}^{\Lambda}|^2 + 4|\tau_{23}^{\Lambda}|^2} \right). \quad (\text{A.5})$$

The corresponding residues are given explicitly in Tab. I.

For the integral Eq. (A.1) one substitutes the 'center of time' $T = t_1 + t_2$ and the 'relative time' $\Delta t = t_2 - t_1$:

$$\int_{t_n}^{t_{n+1}} dt_1 \int_{m_j}^{t_{m+1}} dt_2 \longrightarrow \frac{1}{2} \left[\int_{t_m - t_{n+1}}^{t_{m+1} - t_{n+1}} d\Delta t \int_{2t_m - \Delta t}^{2t_{n+1} + \Delta t} dT + \int_{t_{m+1} - t_{n+1}}^{t_m - t_n} d\Delta t \int_{2t_m - \Delta t}^{2t_{m+1} - \Delta t} dT + \int_{t_m - t_n}^{t_{m+1} - t_n} d\Delta t \int_{2t_n + \Delta t}^{2t_{m+1} - \Delta t} dT \right] \quad (\text{A.6})$$

Res _{ij,n}		ij				ij
		11	22	12	13	33
n	1	$1 + \frac{ \tau_{12}^\Lambda ^2}{(\omega_1 - \omega_2)(\omega_1 - \omega_3)}$	0	0	$\frac{\tau_{12}^\Lambda \tau_{23}^\Lambda}{(\omega_1 - \omega_2)(\omega_1 - \omega_3)}$	Res _{11,n} ($\tau_{12}^\Lambda \rightarrow \tau_{23}^\Lambda$)
	2	$\frac{ \tau_{12}^\Lambda ^2}{(\omega_2 - \omega_1)(\omega_2 - \omega_3)}$	$\frac{\omega_2 - \omega_1}{\omega_2 - \omega_3}$	$\frac{\tau_{12}^\Lambda}{\omega_2 - \omega_3}$	$\frac{\tau_{12}^\Lambda \tau_{23}^\Lambda}{(\omega_2 - \omega_1)(\omega_2 - \omega_3)}$	Res _{12,n} ($\tau_{12}^\Lambda \rightarrow (\tau_{12}^\Lambda)^*$)
	3	$\frac{ \tau_{12}^\Lambda ^2}{(\omega_3 - \omega_1)(\omega_3 - \omega_2)}$	$\frac{\omega_3 - \omega_1}{\omega_3 - \omega_2}$	$\frac{\tau_{12}^\Lambda}{\omega_3 - \omega_2}$	$\frac{\tau_{12}^\Lambda \tau_{23}^\Lambda}{(\omega_3 - \omega_1)(\omega_3 - \omega_2)}$	Res _{13,n} ($\tau_{12}^\Lambda, \tau_{23}^\Lambda \rightarrow (\tau_{12}^\Lambda)^*, (\tau_{23}^\Lambda)^*$)
						23
						Res _{12,n} ($\tau_{12}^\Lambda \rightarrow \tau_{23}^\Lambda$)
						32
						Res _{23,n} ($\tau_{23}^\Lambda \rightarrow (\tau_{23}^\Lambda)^*$)

TABLE I: Residues of Eq. (A.4).

for $t_{n+1} - t_n \geq t_{m+1} - t_m$. The opposite case follows analogously. It proves advantageous to separate the problem into $n = m$ and $n \neq m$. We start with the case $n = m$. With the above substitution one can write the i, j matrix element of Eq. (A.1) in terms of digamma $\Psi(x)$ and hypergeometric functions ${}_2F_1(a, b, c, z)$:³⁶

$$\begin{aligned}
& \left[\int_{t_n}^{t_{n+1}} ds_1 \int_{t_n}^{t_{n+1}} ds_2 G^{\text{ret}}(t_{n+1}, s_1) \Sigma_{\text{res}}^K(s_1, s_2) G^{\text{adv}}(s_2, t_{n+1}) \right]_{ij} = \lim_{\delta \rightarrow 0} \sum_{\substack{\alpha=L,R \\ k,l=1,2,3}} T_\alpha \text{Res}_{i\alpha,k} \text{Res}_{j\alpha,l}^* e^{-i\Delta\omega_{kl}t_{n+1}} \\
& \times \left[\int_{t_n-t_{n+1}}^{-\delta} d\Delta t \int_{2t_n-\Delta t}^{2t_{n+1}+\Delta t} dT + \int_{\delta}^{t_{n+1}-t_n} d\Delta t \int_{2t_n+\Delta t}^{2t_{n+1}-\Delta t} dT \right] \frac{\Gamma}{\sinh(\pi T_\alpha \Delta t)} e^{i\mu_\alpha \Delta t} e^{\frac{1}{2}iT\Delta\omega_{kl}} e^{-i\frac{1}{2}\Delta t(\omega_k + \omega_l^*)} \\
& = \sum_{\substack{\alpha=L,R \\ k,l=1,2,3}} \text{Res}_{i\alpha,k} \text{Res}_{j\alpha,l}^* e^{-i(\omega_k t_{n+1} - \omega_l^* t_{n+1})} \frac{4T_\alpha \Gamma}{i\Delta\omega_{kl}} \left(e^{i\Delta\omega_{kl}t_{n+1}} \left[\frac{1}{2\pi T_\alpha} \left\{ -\Psi\left(\frac{-i\mu_\alpha + i\omega_k + \pi T_\alpha}{2\pi T_\alpha}\right) + \Psi\left(\frac{i\mu_\alpha - i\omega_l^* + \pi T_\alpha}{2\pi T_\alpha}\right) \right\} \right. \right. \\
& - \frac{e^{(-i\mu_\alpha + i\omega_k + \pi T_\alpha)(t_n - t_{n+1})}}{-i\mu_\alpha + i\omega_k + \pi T_\alpha} {}_2F_1\left(1, \frac{-i\mu_\alpha + i\omega_k + \pi T_\alpha}{2\pi T_\alpha}, \frac{-i\mu_\alpha + i\omega_k + \pi T_\alpha}{2\pi T_\alpha} + 1, e^{2\pi T_\alpha(t_n - t_{n+1})}\right) \\
& + \left. \frac{e^{(i\mu_\alpha - i\omega_l^* + \pi T_\alpha)(t_n - t_{n+1})}}{i\mu_\alpha - i\omega_l^* + \pi T_\alpha} {}_2F_1\left(1, \frac{i\mu_\alpha - i\omega_l^* + \pi T_\alpha}{2\pi T_\alpha}, \frac{i\mu_\alpha - i\omega_l^* + \pi T_\alpha}{2\pi T_\alpha} + 1, e^{2\pi T_\alpha(t_n - t_{n+1})}\right) \right] \\
& - e^{i\Delta\omega_{kl}t_n} \left[\frac{1}{2\pi T_\alpha} \left\{ -\Psi\left(\frac{-i\mu_\alpha + i\omega_l^* + \pi T_\alpha}{2\pi T_\alpha}\right) + \Psi\left(\frac{i\mu_\alpha - i\omega_k + \pi T_\alpha}{2\pi T_\alpha}\right) \right\} \right. \\
& - \frac{e^{(-i\mu_\alpha + i\omega_l^* + \pi T_\alpha)(t_n - t_{n+1})}}{-i\mu_\alpha + i\omega_l^* + \pi T_\alpha} {}_2F_1\left(1, \frac{-i\mu_\alpha + i\omega_l^* + \pi T_\alpha}{2\pi T_\alpha}, \frac{-i\mu_\alpha + i\omega_l^* + \pi T_\alpha}{2\pi T_\alpha} + 1, e^{2\pi T_\alpha(t_n - t_{n+1})}\right) \\
& + \left. \frac{e^{(i\mu_\alpha - i\omega_k + \pi T_\alpha)(t_n - t_{n+1})}}{i\mu_\alpha - i\omega_k + \pi T_\alpha} {}_2F_1\left(1, \frac{i\mu_\alpha - i\omega_k + \pi T_\alpha}{2\pi T_\alpha}, \frac{i\mu_\alpha - i\omega_k + \pi T_\alpha}{2\pi T_\alpha} + 1, e^{2\pi T_\alpha(t_n - t_{n+1})}\right) \right] \Bigg), \tag{A.7}
\end{aligned}$$

where one has exploited that for $b > 0$

$$\lim_{x \rightarrow 0^+} \frac{e^{(a+b)x}}{a+b} {}_2F_1\left(1, \frac{a+b}{2b}, \frac{a+b}{2b} + 1, e^{2bx}\right) - \frac{e^{(c+b)x}}{c+b} {}_2F_1\left(1, \frac{c+b}{2b}, \frac{c+b}{2b} + 1, e^{2bx}\right) = \frac{1}{2b} \left\{ -\Psi\left(\frac{a+b}{2b}\right) + \Psi\left(\frac{c+b}{2b}\right) \right\}, \tag{A.8}$$

and defined

$$\Delta\omega_{kl} = \omega_k - \omega_l^*. \tag{A.9}$$

In the indices of the residues in Eq. (A.7) one has to replace $\alpha = L$ by 1 and $\alpha = R$ by 3. For the case $m \neq n$ one analogously finds

$$\begin{aligned}
& \left[\int_{t_n}^{t_{n+1}} ds_1 \int_{t_m}^{t_{m+1}} ds_2 G^{\text{ret}}(t_{n+1}, s_1) \Sigma_{\text{res}}^K(s_1, s_2) G^{\text{adv}}(s_2, t_{m+1}) \right]_{ij} = \frac{1}{\pi} \sum_{\substack{\alpha=L,R \\ k,l=1,2,3}} \text{Res}_{i\alpha,k} \text{Res}_{j\alpha,l}^* e^{-i(\omega_k t_{n+1} - \omega_l^* t_{m+1})} \\
& \times \left[\int_{t_m-t_{n+1}}^{t_{m+1}-t_{n+1}} d\Delta t \int_{2t_m-\Delta t}^{2t_{n+1}+\Delta t} dT + \int_{t_{m+1}-t_{n+1}}^{t_m-t_n} d\Delta t \int_{2t_m-\Delta t}^{2t_{m+1}-\Delta t} dT + \int_{t_m-t_n}^{t_{m+1}-t_n} d\Delta t \int_{2t_n+\Delta t}^{2t_{m+1}-\Delta t} dT \right] \frac{\Gamma e^{i\mu_\alpha \Delta t} e^{\frac{1}{2}iT\Delta\omega_{kl}}}{\sinh(\pi T_\alpha \Delta t)} e^{-i\frac{1}{2}\Delta t(\omega_k + \omega_l^*)} \\
& = \sum_{\substack{\alpha=L,R \\ k,l=1,2,3}} T_\alpha \text{Res}_{i\alpha,k} \text{Res}_{j\alpha,l}^* e^{-i(\omega_k t_{n+1} - \omega_l^* t_{m+1})} \frac{4T_\alpha \Gamma}{i\Delta\omega_{kl}} \\
& \times \left[-e^{i\Delta\omega_{kl}t_{n+1}} \frac{e^{(i\mu_\alpha - i\omega_l^* + \pi T_\alpha)(t_{m+1}-t_{n+1})}}{i\mu_\alpha - i\omega_l^* + \pi T_\alpha} {}_2\mathcal{F}_1\left(1, \frac{i\mu_\alpha - i\omega_l^* + \pi T_\alpha}{2\pi T_\alpha}, \frac{i\mu_\alpha - i\omega_l^* + \pi T_\alpha}{2\pi T_\alpha} + 1, e^{2\pi T_\alpha(t_{m+1}-t_{n+1})}\right) \right. \\
& + e^{i\Delta\omega_{kl}t_{n+1}} \frac{e^{(i\mu_\alpha - i\omega_l^* + \pi T_\alpha)(t_m-t_{n+1})}}{i\mu_\alpha - i\omega_l^* + \pi T_\alpha} {}_2\mathcal{F}_1\left(1, \frac{i\mu_\alpha - i\omega_l^* + \pi T_\alpha}{2\pi T_\alpha}, \frac{i\mu_\alpha - i\omega_l^* + \pi T_\alpha}{2\pi T_\alpha} + 1, e^{2\pi T_\alpha(t_m-t_{n+1})}\right) \\
& - e^{i\Delta\omega_{kl}t_m} \frac{e^{(i\mu_\alpha - i\omega_k + \pi T_\alpha)(t_m-t_{n+1})}}{i\mu_\alpha - i\omega_k + \pi T_\alpha} {}_2\mathcal{F}_1\left(1, \frac{i\mu_\alpha - i\omega_k + \pi T_\alpha}{2\pi T_\alpha}, \frac{i\mu_\alpha - i\omega_k + \pi T_\alpha}{2\pi T_\alpha} + 1, e^{2\pi T_\alpha(t_m-t_{n+1})}\right) \\
& + e^{i\Delta\omega_{kl}t_{m+1}} \frac{e^{(i\mu_\alpha - i\omega_k + \pi T_\alpha)(t_{m+1}-t_{n+1})}}{i\mu_\alpha - i\omega_k + \pi T_\alpha} {}_2\mathcal{F}_1\left(1, \frac{i\mu_\alpha - i\omega_k + \pi T_\alpha}{2\pi T_\alpha}, \frac{i\mu_\alpha - i\omega_k + \pi T_\alpha}{2\pi T_\alpha} + 1, e^{2\pi T_\alpha(t_{m+1}-t_{n+1})}\right) \\
& + e^{i\Delta\omega_{kl}t_m} \frac{e^{(i\mu_\alpha - i\omega_k + \pi T_\alpha)(t_m-t_n)}}{i\mu_\alpha - i\omega_k + \pi T_\alpha} {}_2\mathcal{F}_1\left(1, \frac{i\mu_\alpha - i\omega_k + \pi T_\alpha}{2\pi T_\alpha}, \frac{i\mu_\alpha - i\omega_k + \pi T_\alpha}{2\pi T_\alpha} + 1, e^{2\pi T_\alpha(t_m-t_n)}\right) \\
& - e^{i\Delta\omega_{kl}t_{m+1}} \frac{e^{(i\mu_\alpha - i\omega_k + \pi T_\alpha)(t_{m+1}-t_n)}}{i\mu_\alpha - i\omega_k + \pi T_\alpha} {}_2\mathcal{F}_1\left(1, \frac{i\mu_\alpha - i\omega_k + \pi T_\alpha}{2\pi T_\alpha}, \frac{i\mu_\alpha - i\omega_k + \pi T_\alpha}{2\pi T_\alpha} + 1, e^{2\pi T_\alpha(t_{m+1}-t_n)}\right) \\
& - e^{i\Delta\omega_{kl}t_n} \frac{e^{(i\mu_\alpha - i\omega_l^* + \pi T_\alpha)(t_{m+1}-t_n)}}{i\mu_\alpha - i\omega_l^* + \pi T_\alpha} {}_2\mathcal{F}_1\left(1, \frac{i\mu_\alpha - i\omega_l^* + \pi T_\alpha}{2\pi T_\alpha}, \frac{i\mu_\alpha - i\omega_l^* + \pi T_\alpha}{2\pi T_\alpha} + 1, e^{2\pi T_\alpha(t_{m+1}-t_n)}\right) \\
& \left. - e^{i\Delta\omega_{kl}t_n} \frac{e^{(i\mu_\alpha - i\omega_l^* + \pi T_\alpha)(t_m-t_n)}}{i\mu_\alpha - i\omega_l^* + \pi T_\alpha} {}_2\mathcal{F}_1\left(1, \frac{i\mu_\alpha - i\omega_l^* + \pi T_\alpha}{2\pi T_\alpha}, \frac{i\mu_\alpha - i\omega_l^* + \pi T_\alpha}{2\pi T_\alpha} + 1, e^{2\pi T_\alpha(t_m-t_n)}\right) \right]. \tag{A.10}
\end{aligned}$$

Similarly one can derive $S^K(t, t)$, which additionally involves the trigamma function $\Psi(1, x)$.

-
- ¹ S. Andergassen, V. Meden, H. Schoeller, J. Splettstoesser, and M.R. Wegewijs, *Nanotechnology* **21**, 272001 (2010).
² A. Hewson, *The Kondo Problem to Heavy Fermions* Cambridge University Press, Cambridge, 1993.
³ P. Schlottmann, *Phys. Rev. B* **22**, 613 (1980); *ibid.* **25**, 4815 (1982).
⁴ V. M. Filyov and P. B. Wiegmann, *Phys. Lett.* **81A**, 175 (1980).
⁵ H. Schoeller and J. König, *Phys. Rev. Lett.* **84**, 3686 (2000).
⁶ A. Rosch, J. Paaske, J. Kroha, and P. Wölfle, *Phys. Rev. Lett.* **90**, 076804 (2003).
⁷ P. Schmitteckert, *Phys. Rev. B* **70**, 121302(R) (2004).
⁸ F.B. Anders and A. Schiller, *Phys. Rev. Lett.* **95**, 196801 (2005).
⁹ F.B. Anders and A. Schiller, *Phys. Rev. B* **74**, 245113 (2006).
¹⁰ S. Weiss, J. Eckel, M. Thorwart, and R. Egger, *Phys. Rev. B* **77**, 195316 (2008).
¹¹ T.L. Schmidt, P. Werner, L. Mühlbacher, and A. Komnik, *Phys. Rev. B* **78**, 235110 (2008).
¹² H. Schoeller, *Eur. Phys. J. Spec. Top.* **168**, 179 (2009).
¹³ F. Heidrich-Meisner, A.E. Feiguin, and E. Dagotto, *Phys. Rev. B* **79**, 235336 (2009).
¹⁴ S. Kehrein, *The Flow Equation Approach to Many-Particle Systems* (Springer Verlag, Berlin, 2010).
¹⁵ M. Moeckel and S. Kehrein, *Phys. Rev. Lett.* **100**, 175702 (2008).
¹⁶ M. Pletyukhov, D. Schuricht, and H. Schoeller, *Phys. Rev. Lett.* **104**, 106801 (2010).
¹⁷ C. Karrasch, M. Pletyukhov, L. Borda, and V. Meden, *Phys. Rev. B* **81**, 125122 (2010).
¹⁸ R. Bulla, T. Costi, and Th. Pruschke, *Rev. Mod. Phys.* **80**, 395 (2008).

- ¹⁹ W. Metzner, M. Salmhofer, C. Honerkamp, V. Meden, and K. Schönhammer, *Rev. Mod. Phys.* **84**, 299 (2012).
- ²⁰ S. G. Jakobs, M. Pletyukhov, and H. Schoeller, *Phys. Rev. B* **81**, 195109 (2010).
- ²¹ C. Karrasch, S. Andergassen, M. Pletyukhov, D. Schuricht, L. Borda, V. Meden, and H. Schoeller, *Europhys. Lett.* **90**, 30003 (2010).
- ²² D.M. Kennes, S.G. Jakobs, C. Karrasch, and V. Meden, *Phys. Rev. B* **85**, 085113 (2012).
- ²³ B. Doyon, *Phys. Rev. Lett.* **99**, 076806 (2007).
- ²⁴ L. Borda, K. Vladar, and A. Zawadowski, *Phys. Rev. B* **75**, 125107 (2007).
- ²⁵ E. Boulat, H. Saleur, and P. Schmitteckert, *Phys. Rev. Lett.* **101**, 140601 (2008).
- ²⁶ P. Mehta, and N. Andrei, *Phys. Rev. Lett.* **96** 216802 (2006); P. Mehta, S-P Chao and N. Andrei, [arXiv:cond-mat/0703426](#) (Erratum).
- ²⁷ S. Andergassen, M. Pletyukhov, D. Schuricht, H. Schoeller, and L. Borda, *Phys. Rev. B* **83**, 205103 (2011); *ibid.* **84**, 039905(E) (2011).
- ²⁸ A. Branschädel, E. Boulat, H. Saleur, P. Schmitteckert, *Phys. Rev. B* **82**, 205414 (2010).
- ²⁹ A. Branschädel, E. Boulat, H. Saleur, P. Schmitteckert, *Phys. Rev. Lett.* **105**, 146805 (2010).
- ³⁰ L. Borda, A. Schiller, and A. Zawadowski, *Phys. Rev. B* **78**, 201301 (2008).
- ³¹ V. Kashcheyevs, C. Karrasch, T. Hecht, A. Weichselbaum, V. Meden, and A. Schiller, *Phys. Rev. Lett.* **102**, 136805 (2009).
- ³² D.M. Kennes and V. Meden, *Phys. Rev. B* **85**, 245101 (2012).
- ³³ H. Haug and A.-P. Jauho, *Quantum kinetics in transport and optics of semiconductors* (Springer Verlag, Berlin, 2008).
- ³⁴ J. Rammer, *Quantum Field Theory of Non-equilibrium States* (Cambridge University Press, Cambridge, 2007).
- ³⁵ D.M. Kennes, Master thesis, RWTH Aachen University (2011).
- ³⁶ M. Abramowitz and I.A. Stegun, *Handbook of Mathematical Functions* (Dover, New York, 1965).
- ³⁷ Without any approximations the high energy cutoff appears naturally. In the derivation of the analytical Eq. 26 we neglected terms of the order $1/\Gamma^2$ which now makes it necessary to introduce the high energy cutoff as an upper bound of integration by hand.
- ³⁸ Y. Meir and N.S. Wingreen, *Phys. Rev. Lett.* **68**, 2512 (1992).
- ³⁹ E. Boulat and H. Saleur, *Phys. Rev. B* **77**, 033409 (2008).
- ⁴⁰ P. Murphy, S. Mukerjee, and J. Moore, *Phys. Rev. B* **78**, 161406 (2008).
- ⁴¹ B. Kubala, J. König, and J. Pekola, *Phys. Rev. Lett.* **100**, 066801 (2008).
- ⁴² T. A. Costi and V. Zlatić, *Phys. Rev. B* **81**, 235127 (2010).
- ⁴³ S. Andergassen, T. A. Costi and V. Zlatić, *Phys. Rev. B* **84**, 241107(R) (2011).